HIGH-RESOLUTION THREE-DIMENSIONAL SEISMIC IMAGING OF THE BAIKAL AND AMUR REGIONS OF EASTERN RUSSIA

Haijiang Zhang[1, 2], Kevin G. Mackey[3], Kazuya Fujita[3], Lee K. Steck[4], Charlotte A. Rowe[4], Clifford H. Thurber[1], and Steven Roecker[5]

University of Wisconsin-Madison[1], Massachusetts Institute of Technology[2], Michigan State University[3], Los Alamos National Laboratory[4], and Rensselaer Polytechnic Institute[5]

Sponsored by National Nuclear Security Administration
Office of Nonproliferation Research and Development
Office of Defense Nuclear Nonproliferation

Contract No. DE-FC52-06NA27325[1–4]

ABSTRACT

Eastern Russia is composed of a series of allochthonous terranes which have accreted to the Precambrian Siberian (North Asian) craton. This study is focused on the southern part (Baikal and Amur regions), where accretionary terranes form a suture zone between the Siberian and North China cratons, which is being exploited by the present-day boundary between the Eurasian plate and the Amur block. The complexities of accretion and subsequent intracontinental deformation likely result in a highly heterogeneous crust, a broad zone of deformation, and the formation of small blocks within the ancient suture and present-day plate boundary zones. We assembled catalog picks from ~13000 events and ~100 stations for the Baikal and Amur regions in the period of 1970 to 2005. Using the double-difference tomography method (Zhang and Thurber, 2003, 2006), our study for the first time provides a detailed seismic velocity model of the crust and upper mantle for this complicated area.

The original sources for the Siberia database vary from published Siberia-wide Russian earthquake bulletins to unpublished bulletins of regional network operators. It is very likely that there still exist some arrival time pick outliers in the assembled data. Quality assessment of picks and event-pair differential times is a critical aspect for achieving a high-quality velocity model for the Baikal and Amur regions. In our study we identify and remove outliers in catalog picks using event-pair differential times based on the fact that travel times from two nearby events should be consistent. In our data set, many arrivals at larger distances are identified in the catalog as Pg or Sg phases, which are often observable because of their relatively large amplitudes. To use the double-difference tomography method that is based on first arrivals, we adopt a simple strategy to remove secondary Pg and Sg picks. When the epicentral distance is greater than the estimated crossover distance of 130 km, only Pn and Sn phases are selected.

In our tomography algorithm, we use a spherical-Earth finite-difference (SEFD) travel time method to calculate travel times and trace rays. The basic concept is the extension of a standard Cartesian FD travel time algorithm (Vidale, 1990) to the spherical case through development of a mesh in radius, co-latitude, and longitude, expression of the finite difference (FD) derivatives in a form appropriate to the spherical mesh, and the construction of "stencils" to calculate extrapolated travel times. We benchmark the SEFD method against the "sphere-in-a-box" Cartesian FD travel time algorithm (Flanagan et al., 2007). To improve the accuracy and efficiency of the ray tracing, we adopt a hybrid approach. First, we utilize the FD method with a coarser grid interval to calculate an approximate ray path. Next we start bending this approximate ray path with the spherical pseudo-bending approach of Koketsu and Sekine (1998) until it converges to the desired accuracy.

Our preliminary Vp and Vs models show that at shallow depths (5–10 km), some model anomalies correlate relatively well with local geologic features. For example, the Upper Angara (northeast of Baikal) and Tunka (southwest of Baikal) basins show as strong low-velocity regions. At a depth of 110 km, the low velocities follow the active rift zone in the west and the presumed region of the present-day plate boundary in the east, possibly due to transtensional segments along the Amur-Eurasia boundary.

OBJECTIVES

The objectives of this project are to investigate and develop new and improved methodologies for regional-scale three-dimensional (3D) seismic tomography using a combination of event- and station-pair arrival time differences, and to apply the new methods to the Michigan State University (MSU) and Los Alamos National Laboratory (LANL) Siberia database. The tomographic work proposed here will provide a more reliable velocity model for both the crust and upper mantle of the accretionary regions to the south and east of the Siberian craton. There are four main tasks in this project: (1) an extension of our development of double-difference (DD) seismic tomography to the use of station-pair residual differences, including incorporation of a new method for resolution matrix calculation; (2) testing, refinement, and adaptation of a method for SEFD travel time calculations for use in DD tomography; (3) an extension of our Cartesian adaptive-grid DD tomography algorithm to spherical coordinates; and (4) collaborative work among the UW-Madison, LANL, and MSU groups to apply these analysis tools to the Siberia data set. In the 1st year of this project, our focus is to assemble a data set for the Baikal and Amur regions, incorporate a new resolution estimation method based on an approximate singular value decomposition (SVD) (Zhang and Thurber, 2007), refine and incorporate the SEFD travel time calculation method in our existing DD tomography code, and determine 3D P- and S-wave velocity models for the Baikal and Amur regions.

Figure 1 shows a schematic map of the study area showing primary tectonic features. The study area lies at the southern edge of the Siberian platform (North Asian Craton) and incorporates the suture between it and the terranes that form northern China (Figure 1). This suture closed in roughly mid-Mesozoic time. The present-day boundary between the Eurasia plate and the Amur block (or microplate) is exploiting this older zone of weakness and is represented by the extensional Baikal rift system (west of 120°E) and the Stanovoi fold belt (primarily strike-slip, east of 120°E). It is generally thought that the Baikal rift system is a far field effect of the India collision, although this is contentious.

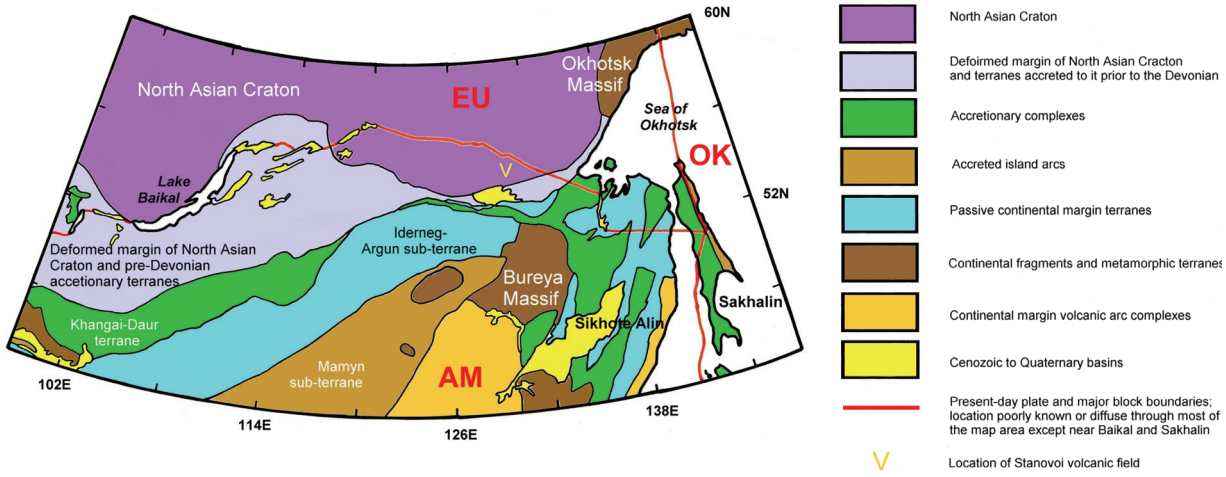

Figure 1. Tectonic map showing terranes and present-day plate boundaries in the study area. Terranes are grouped by tectonic origin. Red lines show approximate present-day plate and major block boundaries. EU = Eurasian plate, OK = Okhotsk block, AM = Amur block. V denotes location of Stanovoi Volcanic field. Simplified and modified after Parfenov et al. (1999, 2003).

RESEARCH ACCOMPLISHED

Data Collection and Quality Control

We have assembled a data set for the Baikal and Amur regions in the area of 45° to 60° latitude and 100° to 145° longitude from the MSU Siberia database. There are ~49000 P (Pg+Pn) and ~82000 S (Sg+Sn) phases corresponding to ~13000 events and ~100 stations. For each event, there are at least 4 observations. Figure 2 shows composite travel curve for Pg, Pn, Sg, and Sn phases using the original catalog locations. We found that many arrivals at larger distances are actually Pg or Sg phases because of their relatively large amplitudes. To use the DD

tomography method that is based on first arrivals, we adopted a simple strategy to remove secondary Pg and Sg picks. When the epicentral distance is greater than the estimated crossover distance of 130 km, only Pn and Sn phases are selected. At the first phase of simultaneous determination of event locations and velocity models, we also require there to be at least 8 observations available for each event. After this process, ~9300 P and ~7200 S phases are selected for ~1250 events (Figure 3).

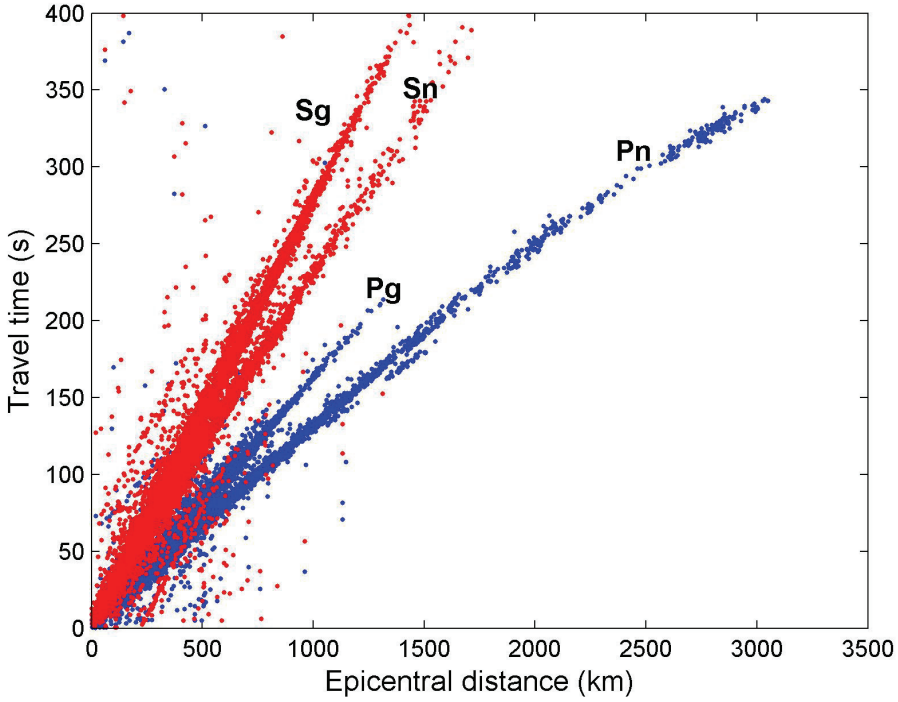

Figure 2. Composite travel time curve for Baikal and Amur regions. The epicentral distance is calculated using original Russian catalog locations.

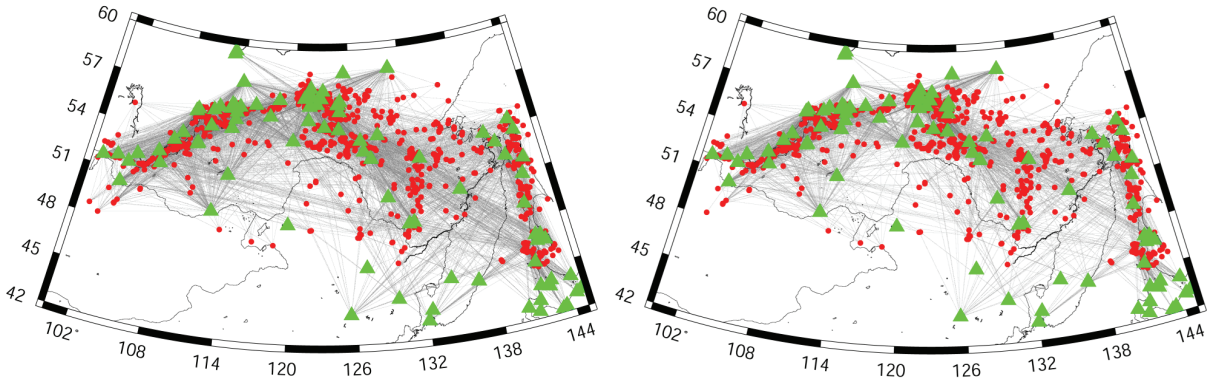

Figure 3. Event-station path coverage for P-waves (left) and S-waves (right). There are ~16500 paths from ~1250 events (red dots) and ~100 stations (green triangles).

The original sources for the MSU Siberia database vary from published Siberia-wide Russian earthquake bulletins to unpublished bulletins of regional network operators. As shown in Figure 2, it is very likely that there still exist some arrival time pick outliers in the assembled data. Quality assessment of picks and event-pair differential times is obviously a critical aspect for achieving a high-quality velocity model of the Siberia region. Here we report our strategy to identify outliers in catalog picks using event-pair differential times.

For each event pair, we calculate the absolute values of catalog differential P (or S) travel times at available stations and then calculate their average values (*ave*) and standard deviations (δ). At each station, we check to see if the absolute value of the differential time is within a specified range that is determined by *ave* + *C*δ. Because of different distances and azimuths from different stations to the event pair, the differential times may vary significantly due to strong source region heterogeneity. For this reason, we intentionally set the scale parameter *C* to be relatively large in order to simultaneously identify outliers and keep useful information. If the differential time is out of range at one station, then we flag the picks from these two events at this station as likely outliers. We then continue this process for all pairings of events and count the number of outlier flags for each pick. If it is greater than a specified threshold (*thr*), this pick will be removed from the data set. Both the scale parameter *C* and the threshold *thr* need to be tested to find appropriate values. For this data set, we select C to be 4 for P arrivals and 3 for S arrivals and *thr* to be 5. As a result, ~210 P and ~140 S phases are removed.

SEFD Travel Time Calculation

We tested the SEFD code developed by S. Roecker based on an analytical velocity model $V=V_0 (r_0/r)$, where V_0=4.0 km/s, r_0 is the Earth's radius and r is the distance between the source and receivers on the Earth's surface. Figure 4a shows the analytical travel times for a source located at latitude 21.2° and longitude 121.75°. We found that the travel-time errors for the SEFD method could be large near the source region when the grid interval is coarse. To deal with this inaccuracy problem near the source region, we test a multiple-grid strategy, in which a fine grid is used near the source region and a coarse one is used outside the source region. The travel-time field files for different grids are saved and loaded up appropriately if required. The tests show that this strategy improves the travel-time accuracy near the source region and can also potentially decrease the travel-time error accumulation away from the source region (Figure 4b).

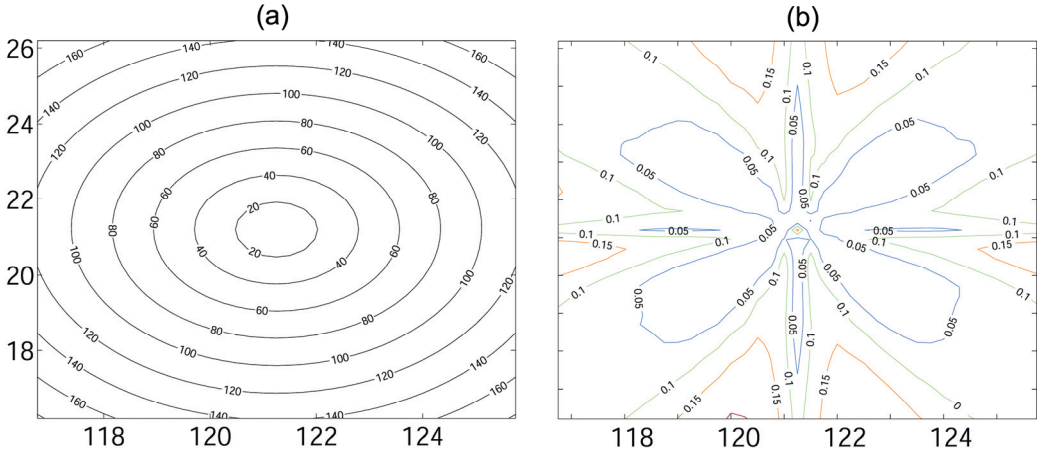

Figure 4. (a) Analytical travel-time contours for a source located at latitude 21.2° and longitude 121.75° based on the velocity model $V=V_0 (r_0/r)$. (b) Travel-time error contours between the SEFD method and analytical solutions. Here a multigrid approach is used to improve the accuracy near the source region (within 30 km). Grid interval is 10 km outside the source region and 1 km in the source region.

Hybrid Ray Tracer

During the reporting period, we successfully developed and tested a hybrid ray tracer combining the spherical pseudo-bending ray tracer of Koketsu and Sekine (1998) and the finite-difference travel time calculation method (Vidale, 1988; Hole and Zelt, 1995; Podvin and Lecomte, 1991) to calculate travel times and ray paths. It is known that in the case of strong heterogeneity, the pseudo-bending algorithm may fail to find the true two-point ray path because of non-linearity of the two-point problem. For this reason, we combine the finite-difference travel time calculation method with the pseudo-bending method in a way that the former provides an approximate ray path for the latter to start with and improve upon. The finite-difference travel time calculation method is capable of computing travel times to all points in the model and can locate diffractions in ray shadow zones. Therefore, it is stable and can find the correct solution even in a strongly heterogeneous medium. However, its accuracy depends on

the grid spacing size, and computation time may be unacceptable if accurate travel times are required. By combining the two methods, however, we can calculate ray paths accurately and efficiently.

Velocity Models of Baikal and Amur Regions

We directly constructed ~53700 P and ~40000 S event-pair differential times using the catalog times. For each event pair, there are at least 4 common observations and the average value is 9. Based on catalog locations, the inter-event distance for each event pair is required to be less than 200 km with an average value of 42 km. Because this is a rather complicated and large area, we tried using 4 different initial 1D models (Figure 5). Model 1 is based on the Quartz DSS line in the west Siberian basin (Morozov et al., 2005) and may not be applicable to the Siberian Platform proper. Model 2 is a mean "Eastern Siberian Platform" model that is based on data from both the Craton and Rift DSS lines (e.g., Egorkin et al., 1988; Cipar et al., 1993), as well as more local work (e.g., Kuznetsov and Titarenko, 1988). The DSS lines are the only ones that are long enough to sample the sub-lithospheric mantle. Compared to Model 1, Model 2 has a higher crustal velocity, a much sharper discontinuity at the Moho, and a smaller gradient through the upper mantle. Model 3 is a "Baikal Rift" model that represents the area under the active rift (Gao et al., 1994; Mishen'kin et al., 1999; and others). Model 4 is a "Southern Baikal" model that averages Primoria, Amur, and parts of eastern Baikal (e.g., Argentov et al., 1976; Mishen'kin et al., 1987; Song et al., 1996). The velocities below 70 km in Models 3 and 4 are the same as used in Model 2 as there have been no long-range profiles south and east of Baikal. The inversion grid intervals are 1 and 2 degrees in latitude and longitude, respectively. The grid nodes are located at depths of 0, 5, 10, 15, 20, 25, 30, 35, 40, 50, 60, 70, 80, 90, 100, 110, 120, 130, and 150 km. Because of potentially significant errors in the catalog arrivals, we applied a large smoothing weight of 200 to the double-difference tomographic system. The initial RMS arrival time residuals for the 4 starting models are 1.612, 1.617, 1.725, and 1.611 s, respectively. The final RMS arrival time residuals are 375, 380, 372, and 365 ms, respectively. The 4 final velocity models show very similar features, as also indicated by comparable final RMS arrival time residuals. Based on both initial and final RMS residuals, however, the velocity models calculated using Model 4 ("Southern Baikal"), which is presumed to represent a large portion of the sampled study area, is the best. Since Vp and Vs models share many similar features, we only present Vp models in the following sections.

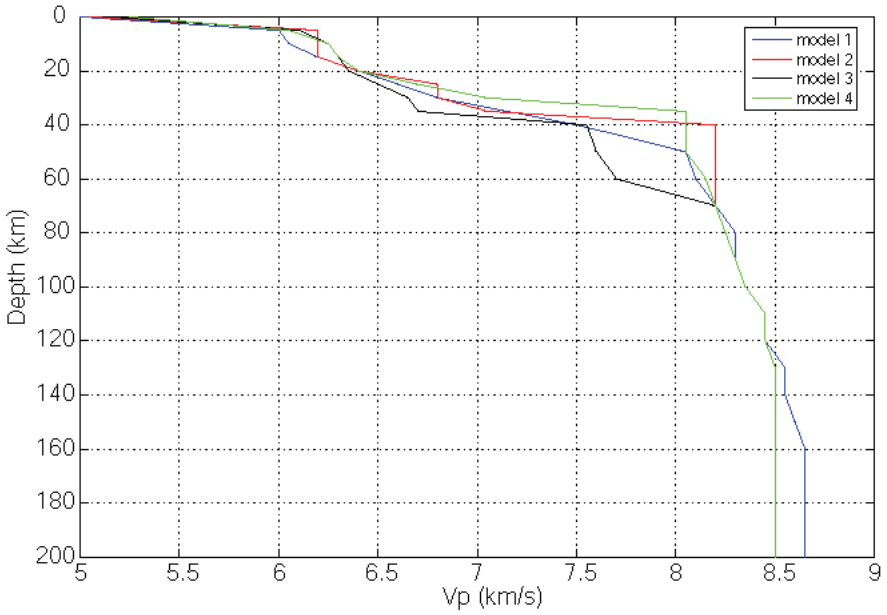

Figure 5. Four different 1D starting models for seismic tomography.

During inversion, we simultaneously determine earthquake locations and velocity models. Figure 6 shows the depth-frequency distribution for ~1250 relocated earthquakes. The number of earthquakes gradually increases at shallow depths and peaks around 10 km and then starts to decrease until at the depth of ~32 km. Most of

earthquakes are located at depths of 5 km to 25 km. Deverchere et al. (2001) also reported a similar depth range of earthquake locations in the Baikal rift, but with a peak distribution around 18 km. They also found some earthquakes occurring as deep as ~50 km. We argue that their earthquake locations are based on 1D Vp and Vs models and large errors could be caused by strong velocity heterogeneities in the Baikal rift. The depth distribution of earthquakes along longitude is similar across different geological features from west to east (Figure 6). Based on more accurate 3D velocity models our study provides more accurate depth estimation for earthquakes, which is very useful to infer the rheological state of the seismogenic layer and the brittle/ductile transition zone.

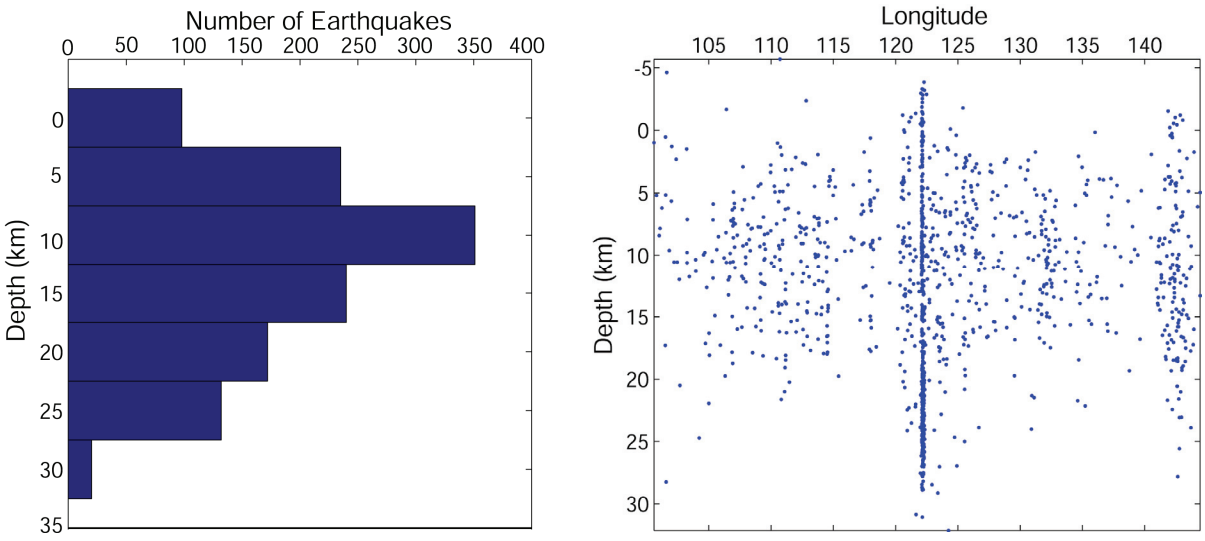

Figure 6. (Left) Depth-frequency distribution of relocated earthquakes from double-difference tomography. (Right) Earthquake depth distribution along longitude. The large cluster at 122°E represents the South Yakutian earthquake sequence of 1989.

Figure 7 shows horizontal slices of the 3D Vp model (using starting model 4) at depths of 5, 10, 20, 30, 40 50, 90, and 110 km, respectively. At shallow depths (5–10 km), some model anomalies correlate relatively well with local geology features. The Upper Angara (northeast of Baikal, indicated by 2 in the 5-km depth slice) and Tunka (southwest of Baikal, indicated by 1 in the 5-km depth slice) basins show as strong low-velocity regions. However, in the northern part of Baikal the velocity is very fast. Other models have also indicated that velocities are normal or slightly elevated at shallow depths beneath Lake Baikal proper (Mackey, 1999; Mishen'kin et al., 1999). A gradient from slow (north) to faster (south) velocities seems to mark the edge of the Siberian platform between longitude 126 and 135. To the north of latitude 54, there are finger-like high-velocity anomalies between longitude 117 and 130, which are similar to those shown in the Pg velocity model by Steck et al. (2007). A low-velocity anomaly lies below Sakhalin Island, as found by Mackey (1999) and Steck et al. (2007); although its cause is unclear, it may be associated with residual elevated temperatures from the Early Cenozoic accretionary phase. At the depth of 20 km, we noticed there are many low-velocity anomalies. Analysis of deep seismic sounding lines, as well as of teleseismic receiver functions, have shown low-velocity layers in the crust beneath the Baikal rift zone, early Mesozoic Mongolia-Okhotsk fold areas, and the Siberian platform (e.g., Mishen'kin et al., 1999; Zorin et al., 2002), as well as in the upper mantle (e.g., Egorkin et al., 1988). These low-velocity layers may reflect inhomogeneities in Earth's crust caused by different geological processes.

In general, the shallower sections of the model show greater heterogeneities, as expected from the variable nature of the crust (c.f., Fig. 1); however, no clear relationship is noted between surficial geology and the crustal velocities. In general lower velocities are concentrated in seismically active regions. Some of the low-velocity anomalies at 30–40 km depth in the southeastern part of the study area appear to be elongate in a northeast-southwest orientation, consistent with the strike of major structures and the late Mesozoic–Early Cenonoic subduction in the region.

Compared to the Pn slowness perturbation model from differential Pn tomography (Rowe et al., 2005), overall the depth slice of 40 km shows similar high/low anomaly patterns. For example, both models have a low velocity

anomaly around Sakhalin Island, and they have a band of high-velocity anomalies running from longitude 135/latitude 50 northwestward.

At the depth slices of 90 and 110 km, the low velocities very clearly follow the present-day plate (block) boundaries; the rift in the west and the presumed strike-slip segment to the east. Given that there may be (or have been) transtensional segments of the North China–Eurasia boundary (such as possibly near the Stanovoi volcanics), the low velocities along the plate (block) boundary are reasonable (Gao et al., 1994). The offset of the low-velocity zone at the northeast end of Lake Baikal to the east is associated with the Barguzin and other depressions.

As shown in the cross-section along 53^{o} latitude, there is clearly a low-velocity anomaly under the Baikal rift zone to depths of > 80 km, as proposed by Mishen'kin et al. (1999), although offset to the northwest. P-wave velocity images determined using teleseismic tomography shows that the low-velocity anomaly zone extends down to the mantle transition zone (Zhao et al., 2006; Lebedev et al., 2006). Crustal thickness, as represented by the 7.5 km/s contour, appears relatively constant throughout the entire study area and no sharp transition to velocities above 8.5 km/s is noted.

CONCLUSIONS AND RECOMMENDATIONS

In this study, we assembled a data set comprising first P- and S-wave arrivals for the Baikal and Amur regions of eastern Russia and applied the DD tomography method to obtain 3D Vp and Vs models for this complicated region. A hybrid ray tracer combining the SEFD travel-time calculation algorithm and the spherical pseudo-bending ray tracing is used to efficiently and accurately calculate travel times and find ray paths between events and stations. Outliers in catalog picks are identified and removed using event-pair differential times based on the fact that travel times from two nearby events should be consistent.

Overall, the model shows greater heterogeneities at shallow depths, as expected from the variable and complicated nature of the crust. Some Cenozoic and Quaternary basins such as the Upper Angara (northeast of Baikal) and Tunka (southwest of Baikal) basins around Lake Baikal correlate very well to strong low-velocity anomalies. Low-velocity anomalies in the mantle beneath the Baikal rift zone are clearly imaged in our model. The low velocities in the depth sections of 90 and 110 km follow the active rift zone in the west and the presumed region of the present-day plate boundary in the east, possibly due to transtensional segments along the Amur-Eurasia boundary.

Our current tomographic algorithm only uses first P- and S-wave arrivals. For this reason, many secondary Pg and Sg arrivals cannot be directly used in our seismic tomography. We are modifying the code so that the secondary Pg and Sg phases are also allowed, and as a result, the crust can be better imaged with better ray coverage. The current tomographic model is solved using a regular inversion grid in latitude, longitude, and depth. Next, we will use the adaptive-mesh tomography method based on tetrahedral diagrams to adapt the inverse mesh according to the data coverage.

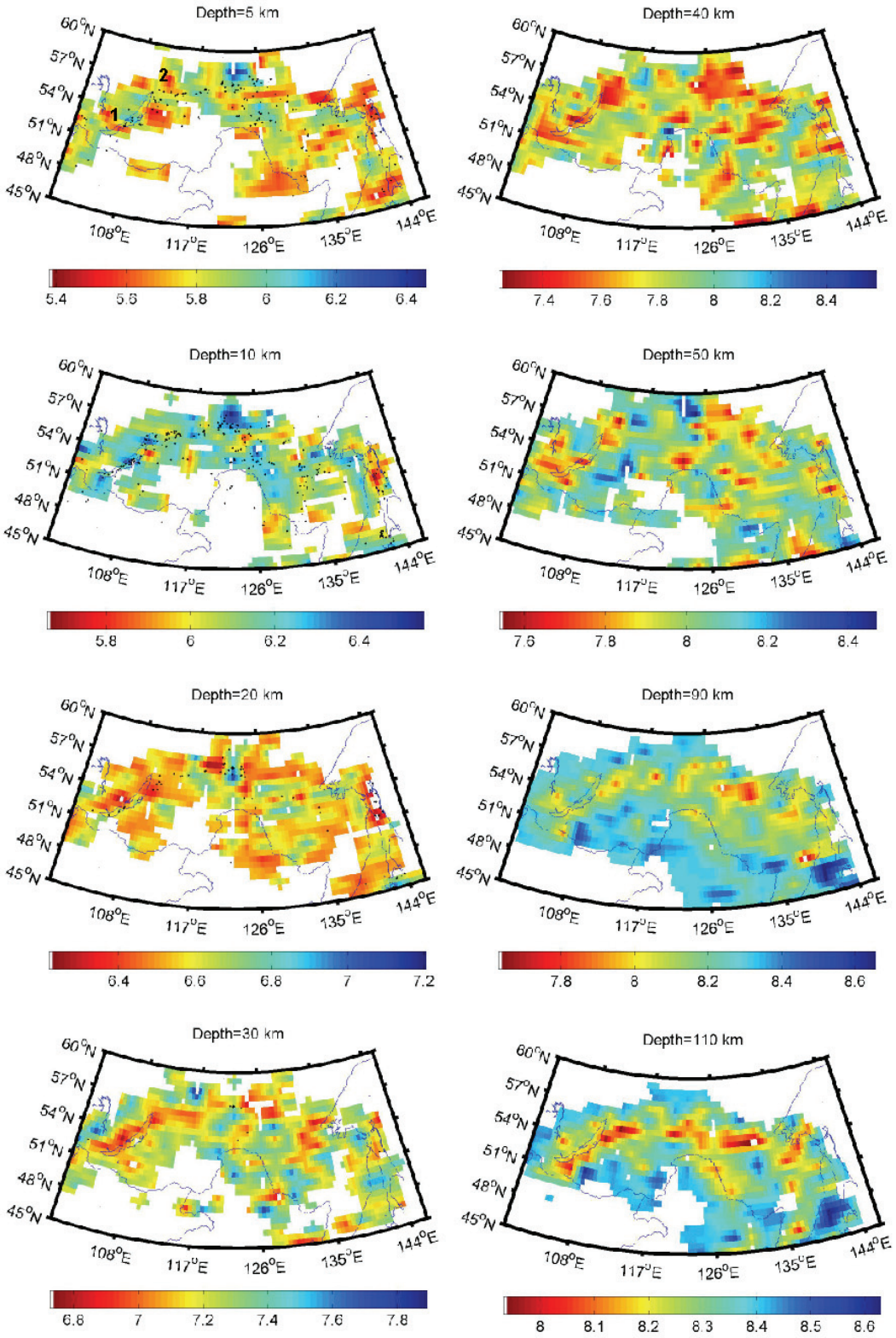

Figure 7. Horizontal slices of the 3D Vp models at depths of 5, 10, 20, 30, 40, 50, 90, and 110 km. In the 5-km slice, 1 denotes Tunka depression; 2 denotes the Upper Angara basin.

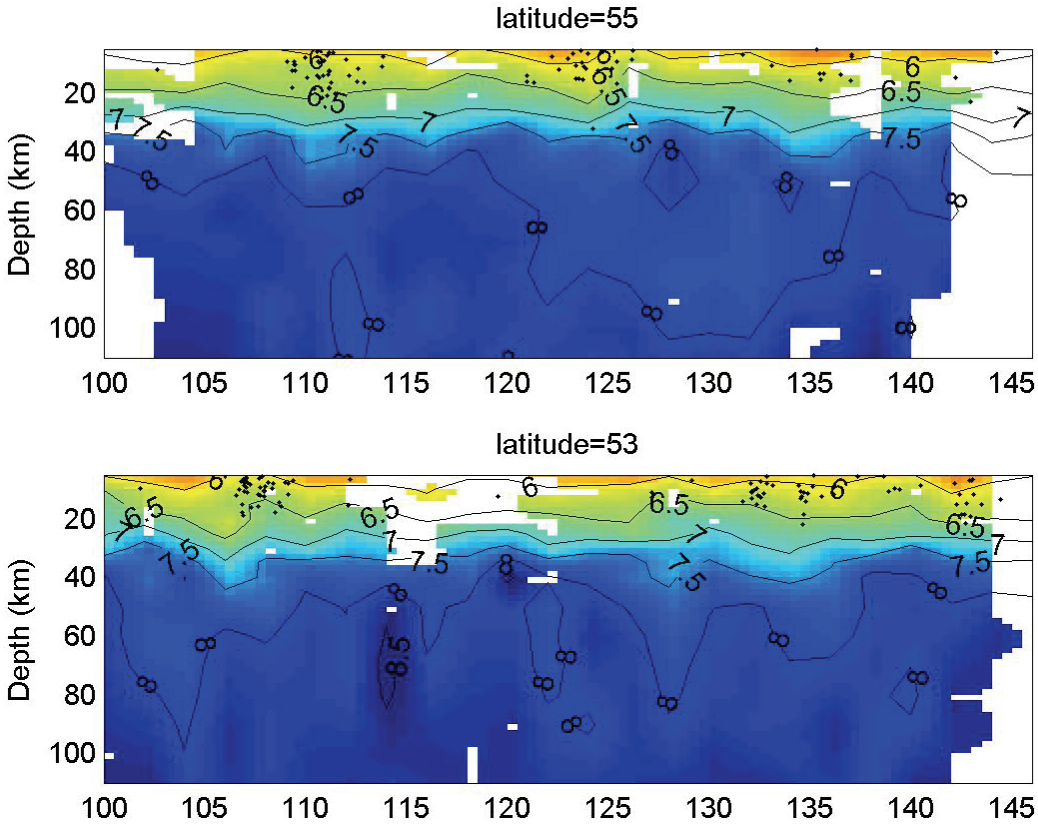

Figure 8. **Cross sections of the 3D Vp model along latitudes of 55° and 53°.**

REFERENCES

Argentov, V. V., G. S. Gnibidenko, A. A. Popov, and S. V. Potap'ev (1976). *Deep structure of Primoria.* Moskow: Nauka (in Russian).

Cipar, J. J., K. Priestley, A. V. Egorkin, and N. I. Pavlenkova (1993). The Yamal Peninsula-Lake Baikal deep seismic sounding profile, *Geophys. Res. Lett.* 20: 1631–1634.

Deverchere, J., C. Petit, N. Gileva, N. Radziminovitch, V. Melnikova, and V. San'kov (2001). Depth distribution of earthquakes in the Baikal rift system and its implications for the rheology of the lithosphere, *Geophys. J. Int.* 146: 714–730.

Egorkin, A. V., S. K. Zyuganov, and N. A. Pavlenkova (1988). Results of investigations of the structure of the lithosphere on profiles in Siberia, *Sov. Geol. Geophys.* 29: 107–114.

Flanagan, M. P., S. C. Myers, and K. D. Koper (2007). Regional travel-time uncertainty and seismic location improvement using a three-dimensional *a priori* velocity model, *Bull. Seism. Soc. Am.* 97: 804–825.

Koketsu, K., and S. Sekine (1998). Pseudo-bending method for three-dimensional seismic ray tracing in a spherical earth with discontinuities, *Geophys. J. Int.* 132: 339–346.

Gao, S., P. Davis, K. Liu, P. Slack, Y. Zorin, N. Logatchev, M. Kogan, P. Burkholder, and R. Meyer (1994). Asymmetric upwarp of the asthenosphere beneath the Baikal rift zone, Siberia, *J.Geophy. Res.* 99: 15319–15330.

Gao, S., K. H. Liu, P. M. Davis, P. D. Slack, Y. A. Zorin, V. Mordvinova, and V. M. Kozhevnikov (2003). Evidence for small-scale mantle convection in the upper mantle beneath the Baikal rift zone, *J. Geophys. Res.* 108: 2194, doi:10.1029/2002JB002039.

Kuznetsov, V. L., and Titarenko, V. V. (1988). Seismic model of the consolidated crust for the western part of the Siberian platform and its articulation zone with the West Siberian plate, *Geol. Geofiz.* 29: 128–135 (in Russian.)

Lebedev, S., T. Meier, and R. D. van der Hilst (2006). Asthenospheric flow and origin of volcanism in the Baikal Rift area, *Earth Planet. Sci. Lett.* 249: 415–424.

Mackey, K. G. (1999). *Seismological Studies in Northeast Russia*, Ph.D. dissertation, Michigan State University, xxiii + 346 pp.

Mishen'kin, B. P., Z. R. Mishen'kina, and V. V. Annenkov (1987). Deep seismic sounding on the Bureya massif, *Geol. Geofiz.* 28: 98–107 (in Russian).

Mishen'kin, B. P., Z .R. Mishen'kina, G. V. Petrik, I. F. Shelud'ko, M. M. Mandel'baum, V. S. Seleznev, and V. M. Solov'ev (1999). Deep seismic sounding of the Earth's crust and upper mantle in the Baikal rift zone, *Izvestiya, Phys. Solid Earth*, 35: 594–611.

Morozov, I. B., E. A. Morozova, S. B. Smithson, P. G. Richards, V. I. Khalturin, and L.N. Solodilov (2005). 3D first-arrival regional calibration model of northern Eurasia, *Bull. Seismol. Soc. Amer.* 95: 951–964.

Parfenov, L .M., L. I, Popeko, and O. Tomurtogoo (1999). The problem of tectonics of the Mongol-Okhotsk region, *Tikhookeans. Geol.* 18: 24–43 (in Russian).

Parfenov, L. M., A. I. Khanchuk, G. Badarch, R. J. Miller, V. V. Naumova, W. J. Nokleberg, M. Ogasawara, A. V. Prokopiev, and H. Yan (2003). Preliminary Northeast Asia geodynamics map, U.S. Geological Survey, Open File Rep. 03-205. Scale 1:5,000,000 (2 sheets).

Podvin, P. and I. Lecomte (1991). Finite difference computation of travel times in very contrasted velocity models: a massively parallel approach and its associated tools, *Geophys. J. Int.* 105: 271–284.

Rowe, C., L. K. Steck, W. S. Phillips, M. Begnaud, R. Stead, and H. Hartse (2005). Pn tomography and location in Eurasia, *2005 IASPEI Meeting* (Santiago, Chile).

Song, Y., S. V. Krylov, B. Yang, L. Cai, S. Dong, T. Liang, J. Li, X. Xu, Z. R. Mishen'kina, G. V. Petrik, I .F. Shelud'ko, V. S. Seleznev, and V. M. Solov'ev (1996). Deep seismic sounding of the lithosphere on the Baikal-northeastern China international transect, *Russ. Geol. Geophys.* 37: 1–13.

Steck, L. K., W. S. Phillips, C. A. Rowe, H. E. Hartse, M. L. Begnaud, R. J. Stead, K. Mackey, and K. Fujita (2007). Pg travel time tomography in Eastern Asia, *Seismol. Res. Lett.* 78: 306.

Vidale, J. (1988). Finite-difference calculation of travel times, *Bull. Seis. Soc. Am.* 78: 2062–2076.

Zhang, H. and C. H. Thurber (2007). Estimating the model resolution matrix for large-seismic tomography problems based on Lanczos bidiagonalization with partial reorthogonalization, *Geophys. J. Int.* 170: 337–345.

Zhang, H. and C. H. Thurber (2003). Double-difference tomography: The method and its application to the Hayward Fault, California, *Bull. Seism. Soc. Am.* 93: 1875–1889.

Zhang, H. and C. Thurber (2006). Development and applications of double-difference tomography, *Pure and Applied Geophys.* 163: 373–403, doi:10.1007/s00024-005-0021-y.

Zhao, D., J. Lei, T. Inoue, A. Yamada, and S. S. Gao (2006). Deep structure and origin of the Baikal rift zone, *Earth Planet. Sci. Lett.* 243: 681–691.

Zorin, Y. A., V. V.Mordvinova, E. Kh. Turutanov, B. G. Belichenko, A. A. Artemyev, G. L. Kosarev, and S. S. Gao (2002). Low seismic velocity layers in the Earth's crust beneath Eastern Siberia (Russia) and Central Mongolia: Receiver function data and their possible geological implication, *Tectonophysics* 359: 307–327.